Color Properties and Trends of the Transneptunian Objects

A. Doressoundiram
Observatoire de Paris

Hermann Boehnhardt
Max-Planck Institute for Solar System Research

Stephen C. Tegler
Northern Arizona University

Chad Trujillo
Gemini Observatory

The color of transneptunian objects (TNOs) is the first and basic information that can be easily obtained to study the surface properties of these faint and icy primitive bodies of the outer solar system. Multicolor broadband photometry is the only tool at the moment that allows characterization of the entire population that is relevant for statistical work. Using the colors available for more than 170 objects it is possible to get a first glance at the color distribution in the Edgeworth-Kuiper belt. First, results show that a wide color diversity characterizes the outer solar system objects. Transneptunian objects have surfaces showing dramatically different colors and spectral reflectances, from neutral to very red. At least one cluster of objects with similar color and dynamical properties (the red, dynamically cold classical TNOs beyond 40 AU) could be identified. Furthermore, evidence for correlations between colors and orbital parameters for certain objects have been found at a high significance level. Both color diversity and anisotropy are important because they are diagnostic of some physical effects processing the surfaces of TNOs and/or some possible composition diversity. In this paper, we will review the current knowledge of the color properties of TNOs, describe the observed color distribution and trends within the Edgeworth-Kuiper belt, and address the problem of their possible origin.

1. INTRODUCTION

It is now clear that Pluto, Charon, and the ≈1200 known (as of January 2007) transneptunian objects (TNOs) are what remain of an ancient disk of icy debris that did not accrete into a giant, jovian-like planet beyond the orbit of Neptune. By studying TNOs, it is possible to examine the preserved building blocks of a planet, and thereby shed some light on the process of planet building in our solar system as well as extrasolar planetary systems.

A photometric survey is a natural first step in the investigation of TNOs because it is the only kind of survey capable of providing a global view of the transneptunian belt. Specifically, it is possible to obtain accurate magnitudes and colors for all of the known TNOs using 2-m- to 10-m-class telescopes. Accurate magnitudes and colors for a large number of TNOs provide a starting point and context for more in-depth techniques such as spectroscopy and spacecraft flybys. It is also possible to look for statistically significant correlations between colors and other properties of TNOs (e.g., orbital properties). Such correlations may yield insight into the important formation and evolution processes in the outer solar system.

An early expectation was that all TNOs should exhibit the same red surface color. But why were outer-main-belt asteroids and jovian trojans known to exhibit red colors (e.g., see *Degewij and van Houten,* 1979)? In addition, *Gradie and Veverka* (1980) suggested that organic materials — molecules defined by C–H bonds — should readily form at large heliocentric distances and cause redder colors at large heliocentric distances. *Gradie and Tedesco* (1982) discovered a correlation between color and semimajor axis of asteroids, implying that asteroids preserve a record of solar system formative and evolutionary processes at various heliocentric distances, rather than being a chaotic mixture. The extraordinary red color of the early Centaur [5145 Pholus (*Mueller et al.,* 1992)] and TNO [1992 QB1 (*Jewitt and Luu,* 1993)] discoveries seemed to confirm the idea that objects at large heliocentric distances exhibited red surface colors. Transneptunian objects were thought to form over a small

range of distance from the Sun where the temperature in the young solar nebula was the same. The similar temperature suggested that TNOs formed out of the solar nebula with the same mixture of molecular ices and the same ratio of dust to icy material. In addition, their similar formation distance from the Sun suggested that TNOs experienced a similar evolution. For example, the irradiation of surface CH_4 ice by cosmic rays, solar ultraviolet light, and solar wind particles could convert some surface CH_4 ice into red, complex, organic molecules. CH_4 ice was known to exist on the surface of Pluto (*Cruikshank et al.,* 1976). Laboratory simulations supported the conversion of CH_4 ice into complex organic material (e.g., *Moore et al.,* 1983; *Strazzulla et al.,* 1984; *Andronico et al.,* 1987). By their nature, the complex organic molecules were expected to absorb more incident blue sunlight than red sunlight. Therefore, the light reflected from the surfaces of TNOs, and observed on Earth, was expected to consist of a larger ratio of red to blue light than the incident sunlight. It was a surprise, therefore, to discover that TNOs exhibited a wide range of colors.

Dynamically, the Edgeworth-Kuiper belt is strongly structured, and three main populations are usually distinguished within this region. The resonant TNOs are trapped in mean-motion resonances with Neptune, in particular the 2:3 at 39.4 AU (the so-called "Plutinos"), and are usually on highly eccentric orbits. The less-excited classical TNOs, also called "classicals," populate the region between the 2:3 and the 1:2 (say 40 AU < a < 50 AU) resonances. The "scattered disk objects" (SDOs) make up a less-clearly-defined population and are mainly objects with high eccentricity e and perihelion near Neptune that were presumably placed in these extreme orbits by a weak interaction with Neptune. The "Centaurs," finally, represent a dynamical family of objects in unstable orbits with semimajor axes between Jupiter and Neptune. The classification given here is historically the first one adopted by the community, but the frontiers between each group are not easy to define. Moreover, the classicals are a diverse population consisting of objects ranging from low to very high degrees of dynamical excitation. Obviously this population needs to be dissected carefully. A most complete and rigorous classification is discussed in the chapter by Gladman et al.

How do the color properties compare within each dynamical group of TNOs? Answering this question will provide important clues to understand how these objects have been formed and how their surface properties have evolved. Indeed the different orbital properties characterizing each dynamical family of TNO should have a distinct impact on the color properties of the surfaces of TNOs. For example, those objects in extreme orbits (high i and e) experience more energetic collisions than those in circular orbits. Such energetic collisions in turn have a significant impact on resurfacing, thus on the color of the surface.

In the sections that follow, we discuss observational strategies, data reduction techniques, and analysis methods of TNO photometric surveys (section 2), observed optical and near-infrared colors (section 3), correlations between colors and orbital elements (section 4), links between colors and chemical and mineralogical properties of TNOs (section 5), and possible processes responsible for the observed colors of TNOs (section 6).

2. PRINCIPLE AND TOOLS OF TRANSNEPTUNIAN OBJECT PHOTOMETRY

2.1. Observational Strategy

Due to the faintness of the TNOs and Centaurs, it is a very difficult and telescope-time-consuming task to obtain spectroscopy of a statistically representative sample that could be used for in-depth studies of surface properties and their correlations with other physical, dynamical, formation, and evolutionary parameters of the objects. However, a first and much faster (in terms of telescope time) assessment of intrinsic surface properties of these objects is possible through photometric characterization of their reflectance spectra by determining broadband filter colors and spectral gradients derived from the filter measurements. It is assumed that sunlight is reflected at the surfaces of the objects only, and no atmosphere or dust coma is present. Activity induced by intrinsic processes (gas evaporation or cometary activity) or external processes (impacts) is presumed to play a role in the resurfacing of TNOs and Centaurs. In rare cases, such as Pluto (with a tenuous atmosphere) and Chiron (showing episodic cometary activity), the presence of an atmosphere and/or a dust coma may affect the interpretation of the measured colors of the objects.

Since they are well characterized and available at many observatories, astronomical broadband filters are used for the photometric measurements of TNOs and Centaurs, i.e., BVRI for the visible wavelength range and JHK for the near-IR. Due to the faintness of the objects in the respective wavelength range, U and L and M filters can only be used for the very brightest objects (e.g., Pluto-Charon). For the visible, the vast majority of data are available in the Bessel filter set, while only a few measurements are obtained using the Johnson filter set (*Sterken and Manfroid,* 1992, and references therein), which differs from the former one in the transmission ranges of the R and I filters. For the near-IR filter set, the differences in the J_s and K_s transmission ranges compared to standard J and K filters (*Glass,* 1997, and references therein) is of minor importance for color studies of the objects.

Transneptunian objects are challenging to observe because they are faint, move relative to the "fixed" background of stars and galaxies, and exhibit brightness variations (lightcurves). In this section, we discuss these challenges and techniques to overcome them. Note that these problems are reminiscent of the first works performed on main-belt asteroids in the early 1960s and 1970s when available technology at that time did not allow the use of more sophisticated techniques, i.e., spectroscopy (see *McCord and Chapman,* 1975; *Bowell and Lumme,* 1979, and references therein). Then the same logic was applied as

observers progressed from the main belt to Hildas, Trojans (*Hartmann et al.,* 1982), and finally Centaurs and TNOs (*Luu and Jewitt,* 1996).

2.1.1. Faintness. First, the most challenging problem is that the TNO population represents some of the faintest objects in the solar system. The typical apparent visual magnitude of a TNO is about 23 mag, although a few objects brighter than 20 mag are known. Another criterion is the minimum signal-to-noise ratio (SNR) of the photometry: Typically, SNR ~30 (corresponding to an uncertainty of 0.03–0.04 mag) is required to accomplish the spectral classification. Indeed, the differences among the known types of minor bodies (which to first order have the color of the Sun) are much more subtle than for stellar types, so considerably higher photometric accuracy is necessary. The more limited the range of wavelengths, the higher the accuracy needed to distinguish objects of different type. However, to reach such a SNR goal, one needs to overcome two problems: (1) the sky contribution, which could be important and critical for faint objects not only in the infrared, but also for visible observations; and (2) the contamination by unseen background sources such as field stars and galaxies. For instance, the error introduced by a 26-mag background source superimposed on a 23-mag object is as large as 0.07 mag. One solution to alleviate these problems is the use of a smaller aperture for the flux measurement of the object. This method is described in the next section.

2.1.2. Motion relative to background. Transneptunian objects, while at very remote heliocentric distance, still have noticeable motion that restricts the exposures to relatively short integration times. At opposition, the motion of TNOs at 30, 40, and 50 AU are, respectively, about 4.2, 3.2, and 2.63/h, thus producing a trail of ~1.03 in 15 min exposure time in the worst case. The trailing of an object during an exposure has devastating effects on the SNR, since the flux is diluted over a larger area of background sky. This dilution, in turn, introduces higher noise. Thus, increasing exposure time will not necessarily improve the SNR for TNO photometry. For practical purposes, the exposure time is chosen such that the trailing due to the object's motion does not exceed the size of the seeing disk. The observer then takes and combines a number of untrailed exposures to improve the SNR. An alternative is to follow the object at its proper motion. In this case, however, one faces another problem: The point-spread function of the object (PSF) would be obviously different from that of the field stars. Moreover, the so-called aperture correction technique used very frequently for accurate TNO photometry would become very difficult since this method requires the PSF calibration of nearby field stars (see next section).

2.1.3. Lightcurves. The color of a TNO or Centaur is ideally measured simultaneously for the two or more filters in order to guarantee that the same surface area of the object is imaged at the same time. However, the majority of color measurements are obtained by exposing the object through different filters sequentially. In order to avoid color changes induced by albedo and/or shape variations of the likely rotating body, it is important to measure the object flux through the various filters quasi-simultaneously, i.e., within a time interval that is short compared to the rotation period of the object. For instance, for an object with a 10-h rotation period, the phase angle of the surface changes by 10° in 30 min. Hence, very fast rotators can mimic strange surface colors or unexpected color variations [see, e.g., 1994 EV_3 (*Boehnhardt et al.,* 2002)]. Since for many objects the exact rotation period is unknown, it is thus advisable to monitor changes in the object brightness due to rotation by repeated exposures in a single filter (e.g., V filter) intermittent during the complete sequence of filter exposures needed for the color measurement of the object. If the rotation period is known, one can phase the filter exposures to appropriately image the same surface area under the same illumination conditions.

2.2. Data Reduction Techniques

The data reduction consists of the basic reduction steps applicable for the visible and near-IR photometric datasets, i.e., bias and flatfield corrections, cosmic-ray removal, alignment and co-addition of the jittered images, and flux calibration through standard stars.

The brightness of the object is frequently measured through the so-called aperture correction technique (*Howell,* 1989; *Tegler and Romanishin,* 1997; *Doressoundiram et al.,* 2001) as justified by the faintness of the TNOs. The basis of this method is that the photometric measurement is performed by using a small aperture on the order of the size of the seeing disk. Consequently, the uncertainty in the measurement is reduced because less noise from the sky background is included in the aperture. However, by doing so, one loses light from the object. Thus, to determine how much light is thrown away, the so-called "aperture effect" is calibrated using a large number of nearby field stars. This is reasonable as long as the motion of TNOs during each exposure is smaller than the seeing, and hence the TNOs' point-spread functions (PSFs) are comparable to those of field stars. For all the photometry, the sky value can be computed as the median of a sky annulus surrounding the object. The advantages in the use of a small aperture are (1) a decrease of the contribution of the sky, which could be important and critical for faint objects; and (2) a reduction of the risk of contamination of the photometry by unseen background sources.

2.3. Analysis Methods

Many useful physical parameters of TNOs can be derived from broadband photometry. These parameters include color, spectral gradient, absolute magnitude, and size.

2.3.1. Color indices. The color indices used here (such as U–V, B–V, etc.) are the differences between the magnitudes obtained in two filters. In other words, the F_1–F_2 color index (where F_1 and F_2 are any of the UBV, etc., filters) is the ratio of the surface reflectance approximately valid for

the central wavelengths λ_1 and λ_2 of the corresponding filters.

2.3.2. Reflectance spectrum. The information contained in the color indices can be converted into a very-low-resolution reflectance spectrum R_F using

$$R_F = 10^{-0.4\,(M_F - M_F\mathrm{Sun})}$$

where M_F and M_FSun are the magnitudes in filter F of the object and of the Sun, respectively (M_VSun = –26.76). Normalizing the reflectance to 1 at a given wavelength (conventionally, the V central wavelength is used), we have

$$R_{F,V} = 10^{-0.4\,[(M_F - M_V) - (M_F - M_V)\mathrm{Sun}]}$$

The filter magnitudes and colors of the Sun for the filters commonly used can be found in *Hardorp* (1980) and *Degewij et al.* (1980). Values of the main colors for the Sun used here are B–V = 0.67, V–R = 0.36, V–I = 0.69, V–J = 1.03, V–H = 1.36, and V–K = 1.42. Figure 1 illustrates the coarse reflectance spectrum using broadband filter photometry compared to spectroscopy of a TNO.

2.3.3. Spectral gradient. The spectral gradient S is a measure of the reddening of the reflectance spectrum between two wavelengths. It is expressed in percent of reddening per 100 nm

$$S(\lambda_2 > \lambda_1) = (R_{F2,V} - R_{F1,V})/(\lambda_2 - \lambda_1)$$

where λ_1 and λ_2 are the central wavelengths of the F_1 and F_2 filters, respectively. S, given in percent of reddening per 100 nm wavelength difference, is intimately related to the constitution of the surface of the object, although at present it is not possible to draw any detailed conclusions from spectral gradients (or colors) on specific surface properties. By definition, spectral gradient values are a direct measure for the intrinsic reddening of the object produced by the surface properties of the object, i.e., the solar colors are "removed"; hence, S = 0 means exactly solar colors. If several filters are measured over a wider wavelength range (e.g., BVRI to cover the visible spectrum), the spectral gradients can be averaged over the main adjacent color indices (e.g., B–V, V–R, R–I) in order to obtain the overallslope of the reflectance spectrum between the two limiting wavelengths.

2.3.4. Absolute magnitude. The absolute magnitude of a TNO is the magnitude at zero phase angle and at unit heliocentric and geocentric distances. Geometrical effects are removed by reducing the M_F visual magnitude (in the F filter) to the absolute magnitude $M_F(1,1,0)$ using

$$M_F(1,1,0) = M_F - 5\,\log(r\Delta) - \alpha\beta$$

where r, Δ, and α are respectively the heliocentric distance (AU), the geocentric distance (AU), and the phase angle (deg). The term αβ is the correction for the phase brightening effect (*Belskaya and Shevchenko,* 2000; see also the chapter by Belskaya et al.). However, the phase function is

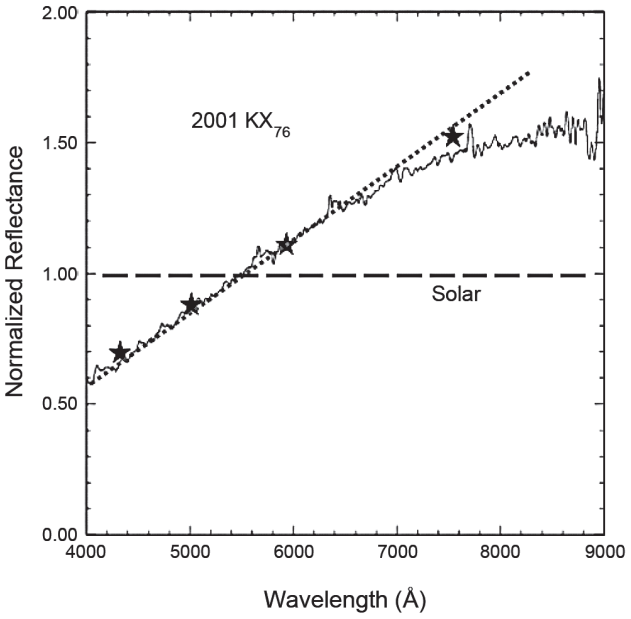

Fig. 1. Reflectance spectrum, broadband filter brightness, and spectral gradient of the TNO 2001 KX_{76} or (28978) Ixion. The reflectance is shown normalized to unity at 550 nm. The BVRI broadband filter brightness is plotted by "star" symbols (from short to long wavelength) over the central wavelength of the respective filter bandpass. The spectral gradient fitted to the spectroscopy and photometry of the object is shown as a dotted line. Neutral/solar reflectance is represented by the dashed line.

completely unknown for most of the TNOs. Based on a first-phase-curve study of a few TNOs, *Sheppard and Jewitt* (2002) have shown almost linear and fairly steep phase curves in the range of phase angles from 0.2° to 2°. They found an average β of 0.15 mag/deg. A similar steep slope was found for Centaurs (*Bauer et al.,* 2002). This implies a possible considerable error in H calculations disregarding the phase correction. Further studies have also been made measuring phase curves in parallel with polarimetry (*Bagnulo et al.,* 2006; *Boehnhardt et al.,* 2004).

2.3.5. Size. Size is the most basic parameter defining a solid body. Unfortunately, sizes (and albedos) are difficult to determine as they mostly require thermal measurements. Hence objects with accurate size determination are few (see chapter by Stansberry et al.). Consequently, for most objects, a canonical geometric albedo p is assumed and the absolute magnitude $M_F(1,1,0)$ can be converted into the radius R of the object (km) using the formula by *Russell* (1916)

$$pR^2 = 2.235 \times 10^{16}\; 10^{0.4(M_F\mathrm{Sun} - M_F(1,1,0))}$$

where M_FSun is the magnitude of the Sun in the filter F (M_VSun = –26.76). Owing to the lack of available albedo measurements, it has become the convention to assume an albedo of 0.04, common for dark objects and cometary nuclei. However, one should be aware of the fact that the sizes

are purely indicative and are largely uncertain. For instance, if we would use, instead, an albedo of 0.14 (i.e., the albedo of the Centaur 2060 Chiron), the results for size estimates would have to be divided by a factor of about 2.

Having these limitations in mind (unconstrained phase function and albedo), in all the following analysis and figures that make use of absolute magnitude and size, we have taken the above values for the phase correction and an average albedo of 0.09 for the geometric albedo (R band).

3. COLOR DIVERSITY AND SPECTRAL GRADIENT

O. Hainaut from the European Southern Observatory in Chile has compiled and maintains a database of color measurements of TNOs, Centaurs, and short-period comets. The database can be accessed at *www.sc.eso.org/~ohainaut/MBOSS*. As of late September 2006, this MBOSS database contains values for 209 objects (Plutinos 32; classicals 95; SDOs 32; Centaurs 30, comets 20) at 1077 epochs covering the UBVRIJHKLM filter set (not all the objects have the full filter set). It also provides references to the values stored. (Note that Tegler and Romanishin have also put colors and magnitudes from their survey for ~120 TNOs and Centaurs on the web at *www.physics.nau.edu/~tegler/research/survey.htm*.)

Both colors and spectral gradients are "integral" characterization parameters of surface properties of the objects: "integral" over the illuminated and visible part of the surface, which for TNOs and distant Centaurs is almost equivalent to a complete hemisphere since the phase angles are small, and "integral" over the wavelength range of the filters used.

3.1. Color-Color Diagrams of Transneptunian Objects

Color-color diagrams show two measured color indices of the object sample vs. each other, e.g., V–R color vs. B–V color as measured for TNOs and/or Centaurs. Solar colors provide the reference for zero intrinsic reddening. Objects with "higher" color indices than solar are called "redder" than the Sun, those with "smaller" values are "bluer" than the Sun. The "redder"/"bluer" colors are equivalent to a positive/negative spectral gradient compared to the solar spectrum. For guidance, the reddening trend line can be drawn in the color-color diagrams: This line connects locations in the color-color diagram with increasing values of constant spectral reflectance slope. Deviations from the reddening trend line indicate a nonlinear behavior of the intrinsic reddening over the spectral range covered by the filters of the color-color diagram. Examples for color-color diagrams of TNOs and Centaurs are shown in Fig. 2.

Color changes over the body's surface combined with rotation of the object can result — in principle — in variations of the object's colors depending on the rotation phase when the measurements are performed (even for simultaneous or quasi-simultaneous filter exposures). For Centaurs in eccentric orbits, changes in the aspect angle due to orbital motion can also result in color variations for objects with nonhomogenous surface colors. (Due to the long orbital periods of TNOs, changes of the aspect angle along the orbit may happen over timescales of decades only, a time interval much longer than the time span during which filter observations of TNOs have been performed up to now.) Similar statements were also made in the 1960s to 1980s when interpreting rotational effects and albedos and colors (see, e.g., *Bowell and Lumme,* 1979; *French and Binzel,* 1989). Rotation phase resolved color measurements of only a few objects are published so far (see chapters by Sheppard et al. and Belskaya et al.). In order to achieve a complete characterization of the color properties of a body, full coverage of the rotation (aspect) phase range is required (but rarely done). In cases where several color measurements are available, averaging of the results can be performed to obtain a mean value for the colors and spectral gradients.

Color-color diagrams of TNOs (as well as of Centaurs and cometary nuclei; see Fig. 2) in the visible show a wide distribution from neutral and even slightly "bluish" to very red values. Figure 2 also shows the various dynamical classes of the TNOs (i.e., classical objects, Plutinos, scattered disk objects) and the Centaurs. All subclasses are color undistinguishable, which is consistent with a common origin for these objects.

For the overall TNO population (of more than 150 objects with BVRI color measurements) clustering is not obvious although originally proposed based upon much smaller samples (*Tegler and Romanishin,* 1998). However, clustering in color-color diagrams is found when considering different populations of TNOs and Centaurs (see discussion below). The trend line overplotted in Fig. 2 represent the locus of object with a linear reflectance spectrum. The "diagonal orientation" of the TNO cloud in the V–R vs. B–V plot in Fig. 2, following the trend line of increased reddening, suggests constant surface reddening from B to R for the majority of the objects. Instead, the respective R–I vs. B–V color-color plot in Fig. 2 clearly indicates systematic deviations from the trend line toward smaller reddening at the long wavelength end of the visible spectrum. In near-IR color-color diagrams (H–K vs. J–H in Fig. 3), a strong clustering of TNOs around solar colors is found that clearly indicates flat and close to neutral surface colors for the majority of the objects. Very few objects show significant reddish colors (*Delsanti et al.,* 2006). Outliers toward bluer than solar colors exist and may be due to absorption bands of surface ices (e.g., H_2O, CH_4) with influence on broadband colors (in particular in H and K filters). In this respect "bluish" near-IR colors may be used to identify potential objects with ice absorption spectra — although the photometric indices are certainly not qualified to replace spectroscopic analysis of the objects for ice signature detections. The changeover from the red color in visible to the more neutral near-IR spectrum in the individual objects happens between about 750 and 1400 nm and thus affects

mostly the I and J filter reflectance. However, it also explains the systematic deviations from the trend lines in R–I vs. B–V color-color diagrams. In other words, visible colors are mutually correlated, while they appear to be unrelated to infrared colors (*Doressoundiram et al.,* 2002; *Delsanti et al.,* 2006).

3.2. Spectral Gradient Histograms of Transneptunian Objects and Centaurs

The full range of spectral gradients of the object sample should be covered by a dense set of [S_{min}, S_{max}] pairs, the lower and upper limit for the spectral gradient of the objects to be counted in the respective histogram bin. Examples for spectral gradient histograms of TNOs and Centaurs are shown in Fig. 4. In the following analysis spectral gradients among TNOs and Centaurs have been obtained from BVRI broadband photometry extracted from the MBOSS database.

The surface characterization by spectral gradients somehow implies and is best used for objects with rather featureless reflectance spectra (i.e., no absorption due to surface ices). This requirement may reasonably be fulfilled in the visible wavelength range where only weak absorption bands are found in a few TNOs (see chapter by Barucci et al.) without noticeable effects on the filter magnitudes. The near-IR wavelength region contains various strong absorption bands of H_2O and CH_4 ices, which have been found in some TNOs. Hence, effects on the surface colors are possible and, indeed, the "bluish" colors J–H and/or J–K may be due to these ice absorptions (see below).

The range of spectral gradients of TNOs and Centaurs in the visible wavelength region ranges from –5%/100 nm to 45%/100 nm, with the exception of some very red Centaurs. The spectral gradient distributions for the four major dynamical classes (classicals, SDOs, Plutinos, and Centaurs) display evident differences (Fig. 4): Classicals cluster between 25 and 35%/100 nm and are abundant also at somewhat smaller reddening slopes (i.e., between 15 and 25%/100 nm). Plutinos and SDOs peak at moderately red levels, while Centaurs show a double peak distribution with a high number at low reddening (5–15%/100 nm, comparable to the range of the distribution maximum for the Plutinos and SDOs) and a shallower peak with very red slopes (35–

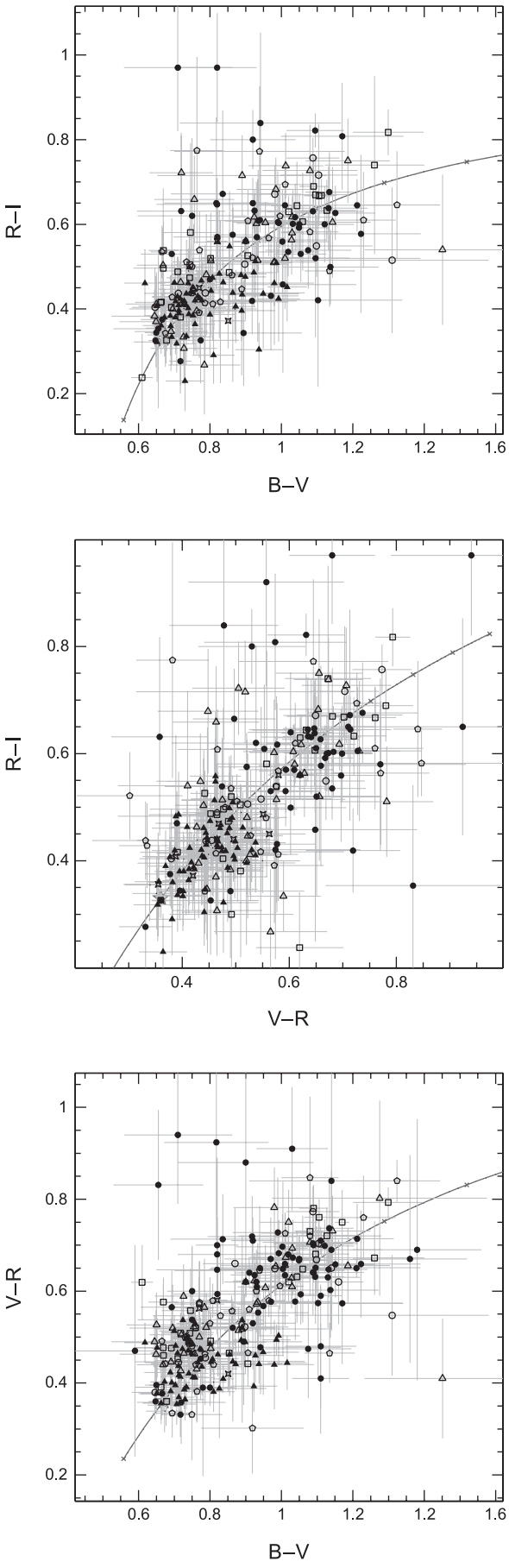

Fig. 2. Color-color diagrams of TNOs (Plutinos = open triangles, classicals = filled circles, SDOs = open pentagons, Centaurs = open squares, Trojans = filled triangles, comets = open four-spike star). The diagrams apply for broadband filter results in BVRI. Solar colors are indicated by an open five-spike star symbol. The curve is the locus of object with a linear reflectivity spectrum. The Sun, as a reference, has a linear reflectivity spectrum with a null slope. A tick mark is placed every 10%/100 nm; the curve is graduated in units of spectral slope from 0 (solar) to 70%/100 nm (very red). Plots are from the web page of O. Hainaut (*www.ls.eso.org/~ohainaut/MBOSS*), who compiles photometric results of minor bodies in the outer solar system.

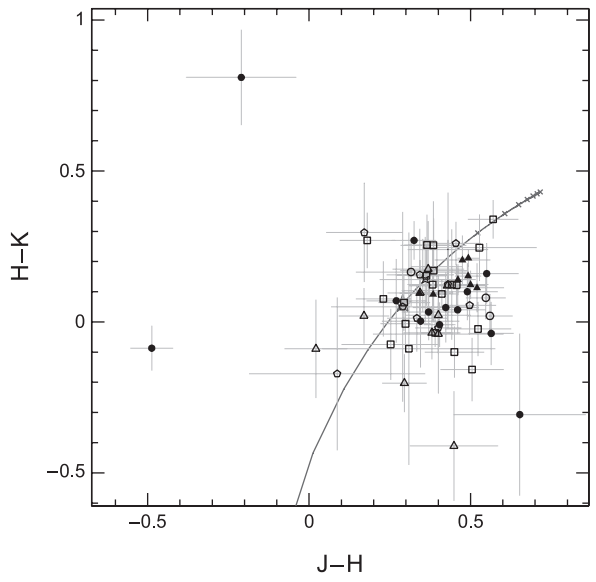

Fig. 3. J–H vs. H–K color-color diagram of TNOs and Centaurs. Symbols are Plutinos = open triangles, classicals = filled circles, SDOs = open pentagons, Centaurs = open squares, Trojans = filled triangles, comets = open four-spike star, Sun = open five-spike star, trend line of increased reddening = solid line. This line is the locus of objects with a reflectivity spectrum of increasing linear slope (see also Fig. 2). Most of the points lie below the reddening curve. This is an indication for a change and decrease of the spectral slope over the JHK range. The two outliers are (19308) 1966 TO_{66} (top left) and (24835) 1995 SM_{55} (bottom left).

45%/100 nm, similar to the main maximum in the classicals histogram). The structured histograms suggest that further subpopulations exist for classicals and Centaurs, which are described and analyzed by more sophisticated statistical methods below. The overall reddening distributions of the TNOs and Centaurs need an interpretation based upon surface processing scenarios and modeling. The spectral gradient in the near-IR wavelength region tend to flatten off (close to solar-type colors are mostly measured) and is not very instrumental for population classification except for the identification and analysis of outliers.

Such analysis is reminiscent of early work done with asteroids in the 1970s and 1980s. In particular, a relation between color (or spectral gradient) and ice abundance in outer solar system objects, as caused by spectral absorption bands, was the background of *Hartmann et al.*'s (1982) work and a subsequent series of papers. These authors showed a direct correlation between position in a V–J vs. J–K diagram, and the measured albedos and ice contents of well-observed satellites and asteroids.

4. COLOR DISTRIBUTION OF THE TRANSNEPTUNIAN OBJECTS: STRONGLY SHAPED

The main purpose is to see if color is a tracer for any physical process. While any physical processes are of interest, we have very little detailed knowledge of physical mechanisms. The physical processes that are easiest to test

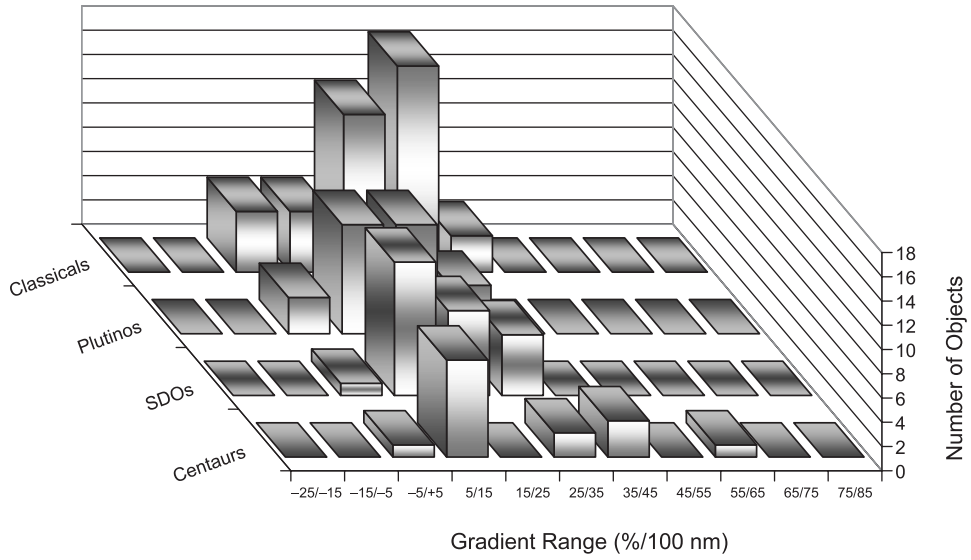

	−25/−15	−15/−5	−5/+5	5/15	15/25	25/35	35/45	45/55	55/65	65/75	75/85
Centaurs	0	0	1	8	0	2	3	0	1	0	0
SDOs	0	0	1	11	7	5	0	0	0	0	0
Plutinos	0	0	3	9	9	4	0	0	0	0	0
Classicals	0	0	5	5	13	17	3	0	0	0	0

Fig. 4. Spectral gradient histogram of TNOs and Centaurs (after *Doressoundiram and Boehnhardt,* 2003).

with such limited knowledge consist of comparisons of color with combinations of orbital physical parameters.

4.1. Database of Colors and Color Indices

For this analysis, we restrict our sample to those collated in the MBOSS database used in the previous section. Here we focus on the visible colors of the TNO surfaces. The analysis is made simpler by the fact that visible colors are mutually correlated throughout the VRI regime (*Boehnhardt et al.,* 2001; *Doressoundiram et al.,* 2002).

This is the basic premise behind the supposition that the coloring agent could be tholin-like materials (*Jewitt and Luu,* 2001; *Cruikshank et al.,* 2005), which tend to produce a uniform color gradient throughout the visible region. This fact allows the transformation of most color values in the MBOSS database to a common reddening scale, the percent of reddening per 100 nm, S (see section 2.3) implemented for the MBOSS database by *Hainaut and Delsanti* (2002). For objects with multiple color values, all are combined into this metric with formal error propagation.

A plot of true V–R vs. the S metric appears in Fig. 5, illustrating that this transformation is valid for objects with multiple color data. The MBOSS database allows us to look at the VRI color characteristics among 176 TNOs and Centaurs listed in the Minor Planet Center database.

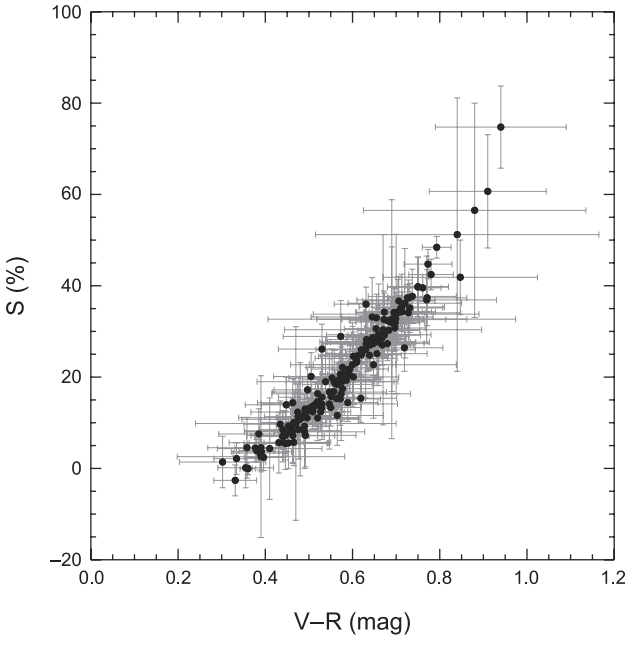

Fig. 5. This plot shows a strong correlation between the reddening factor S (computed in the visible wavelength) and the V–R color of objects. Thus, our transformation of all color data to the common S scale is consistent with measured values of the most common color filter difference, V–R. The use of the S reddening factor allows combinations of all visible colors to be used in correlation analysis and reduces error bars by significant amounts by combining data throughout the VRI wavelength region.

4.2. Correlations

The main purpose of collecting a wide range of color data is to consider whether TNO surface color is related to dynamical factors and can give an indication of how solar system wide factors may impact TNO composition. Plates 1 and 2 are an overview of the color distribution of TNOs obtained within the Meudon Multicolor Survey (2MS) of *Doressoundiram et al.* (2005). The advantage of this view is that it offers to the eye global patterns between color and orbital elements. Although the search for correlations between colors and dynamical information such as orbital elements is open ended, we here limit the search to basic orbital element data and a few derived quantities. The most basic and robust statistical test searching for correlations is the Spearman rank correlation test, which does not presuppose a functional form for the correlation, as do many other statistical tests (*Spearman,* 1904).

4.2.1. Criteria for statistical significance. We compare our color metric S against the most basic of dynamical parameters, orbital elements. Since we are looking for a correlation between color and many potential parameters, we must use a higher criterion for statistical significance than the standard 3σ used throughout astronomy. Indeed, simple simulations show that if a set of 176 uniformly distributed numbers (representing our 176 color values) are compared against n = 6 other uniformly distributed datasets (e.g., representing the 6 basic orbital parameters), a $> 3\sigma$ spurious "correlation" occurs with the Spearman test 1.35% of the time, a factor (n – 1) = 5 in excess of the 0.27% rate expected and seen for comparison to a single orbital parameter.

Therefore, to properly compare color correlations among the orbital parameters, we must raise our threshold to $\approx 3.5\sigma$ for six orbital parameters to realize the 0.27% spurious correlation rate for a 3σ event for a single orbital parameter. Since the probability for spurious correlation increases roughly linearly with the number of extra parameters tested, and Gaussian probabilities are a strong function of σ values, even a moderate increase to 3.8σ is appropriate for considering correlations of up to n = 20 parameters as we do here. We adopt this 3.8σ value here for the remainder of our discussion.

4.2.2. Populations considered. It is quite clear that neither the Plutinos (in the 2:3 mean-motion resonance at 39.4 AU) nor the SDOs (q near Neptune) have any significant correlation between the MBOSS colors and any orbital parameter, and no researchers have reported such correlations. For completeness, we do test the Plutinos and SDOs here. It is also quite clear that Centaurs (q > 5.2 AU and a < 30.1 AU) have a bimodal color distribution of a strength not seen in any TNO population (*Peixinho et al.,* 2003; *Tegler et al.,* 2003; chapter by Tegler et al.). Discussion of the Centaur population is not included in this work as they represent a population that is much more dynamically unstable than the TNOs and is potentially affected by recent cometary activity. Thus, there remain only two populations in the Edgeworth-Kuiper belt that could have any correlation

between color and orbital parameters: the classical TNOs and the "other TNOs," TNOs with semimajor axes in the range (40 AU < a < 50 AU) but with eccentricities too high to be considered classicals. We define this population as the "near-scattered TNOs," since they have similar perihelion properties to the SDOs, but are close enough that the separation between them and the classical TNOs is not easily defined.

It is not easy to determine where the classical TNOs end and the near-scattered TNOs begin. Observers traditionally arbitrarily choose a minimum perihelion value to distinguish between the classical and near-scattered TNOs somewhere between 36 AU and 41 AU. However, dynamical studies have shown that the 40 AU to 50 AU region has many narrow resonances that can mask objects that are true classical TNOs. The *lower limit on the perihelion for discriminating the classical TNO population from the near-scattered TNOs is critical for detecting a color/orbital element correlation* with either population. Evaluating exactly where the perihelion criterion should be set to define classical TNOs is difficult at best and beyond the scope of this work as it is primarily a dynamical argument (see chapter by Gladman et al.). Instead we treat all these TNOs as one class, included in the single denomination of *classical* TNOs, defined as 40 AU < a < 50 AU whatever their eccentricity.

4.2.3. Summary of significant correlations. A statistically significant clustering of very red classical TNOs with low eccentricity (e < 0.05) and low inclination (i < 5°) orbits beyond ~40 AU from the Sun, as first suggested by *Tegler and Romanishin* (2000) from a much smaller dataset, has been confirmed by *Doressoundiram et al.* (2002) and *Trujillo and Brown* (2002). *Doressoundiram et al.* (2002) have shown that this cluster of low-i classical TNOs is statistically distinct from the others classical TNOs (higher i, diverse colors) at the 99% significance level. This red cluster is clearly seen in Plate 1, where objects with perihelion distances around and beyond 40 AU are mostly very red. The cluster members have similar dynamical and surface properties, and they may represent the first taxonomic family in the Edgeworth-Kuiper belt.

Many studies have been performed to search for correlations between color and physical parameters (e.g., size). So far, no significant trend has been found between color and size, or absolute magnitude. This points out that the coloring process (whatever it is) is not sensitive to size, at least in the size range accessible by groundbased observations.

We tested the following four populations: all TNOs (q > 25 AU), the Plutinos (38.5 AU < a < 40 AU), the SDOs (q near Neptune), and the classical TNOs (40 AU < a < 50 AU). These were tested against the following orbital parameters: inclination, eccentricity, perihelion, and the root-mean-square orbit velocity, V_{rms}, as discussed by *Stern* (2002). Indeed, collisional resurfacing could also provide a possible explanation for the orbital element dependency of the color indices: One would naturally expect highly excited objects to suffer more energetic impacts. No other orbital parameters were tested, because no correlations have been reported for other parameters. The results of the correlation tests are shown in Table 1. It is *clear that the entire TNO population shows a statistically significant correlation between color and both rms velocity and inclination*, this trend dominated by the TNOs with 40 AU < a < 50 AU (see Fig. 6), which also show a statistically significant correlation with inclination and rms velocity. There is a moderate color/perihelion correlation for the entire TNO population, but it is at the threshold of significance considering the number of orbital parameters we are testing and is not significant for any subpopulation. Thus, we consider both

TABLE 1. Color correlations.

Population	Correlation Color vs. . . .	N	Significance (Gaussian)	Significance (1 – Conf.)	Significant?
All TNOs (q > 25 AU)	rms velocity	141	5.7σ	1×10^{-8}	Yes
All TNOs (q > 25 AU)	Inclination	141	5.5σ	4×10^{-8}	Yes
All TNOs (q > 25 AU)	Perihelion	141	3.8σ	2×10^{-4}	Maybe
All TNOs (q > 25 AU)	Eccentricity	141	3.1σ	2×10^{-3}	No
Classical TNOs (40 < a < 50 AU)	rms velocity	78	4.5σ	7×10^{-6}	Yes
Classical TNOs (40 < a < 50 AU)	Inclination	78	4.9σ	8×10^{-7}	Yes
Classical TNOs (40 < a < 50 AU)	Perihelion	78	2.5σ	1×10^{-2}	No
Classical TNOs (40 < a < 50 AU)	Eccentricity	78	1.3σ	0.2	No
Scattered (a > 50 AU)	rms velocity	26	1.2σ	0.2	No
Scattered (a > 50 AU)	Inclination	26	1.2σ	0.2	No
Scattered (a > 50 AU)	Perihelion	26	0.6σ	0.5	No
Scattered (a > 50 AU)	Eccentricity	26	1.3σ	0.8	No
Plutinos (38.5 < a < 40 AU)	rms velocity	32	0.0σ	1.0	No
Plutinos (38.5 < a < 40 AU)	Inclination	32	0.0σ	1.0	No
Plutinos (38.5 < a < 40 AU)	Perihelion	32	0.2σ	0.8	No
Plutinos (38.5 < a < 40 AU)	Eccentricity	32	0.1σ	0.9	No

The criterion for statistical significance is set to 3.8σ in this investigation as we tested for correlations between color and 16 different parameter/subpopulation combinations, as explained in the text.

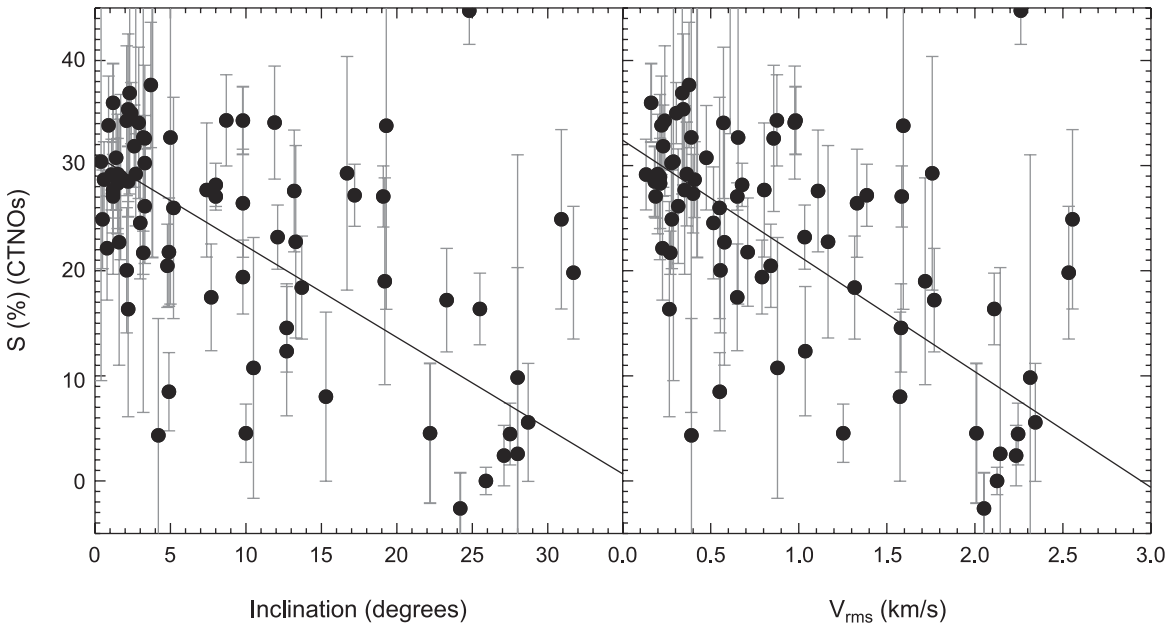

Fig. 6. Color metric S for the classical TNOs vs. inclination and rms orbit velocity V_{rms}. A least-squares linear slope has been fitted to the data to guide the eye. Both of these correlations are significant at the 4σ level using the Spearman test, which does not assume a functional form to the correlation.

the color/inclination and color/rms velocity correlations to be statistically significant.

Although the Spearman rank correlation test excels at determining whether a correlation is statistically significant, it is not useful as a test to determine which correlation is more significant, the inclination or the rms velocity correlation. Thus, it remains to be seen whether a specific testable mechanism can be found that produces either an inclination/color correlation or a rms velocity/color correlation.

5. COLORS AND SURFACE PROPERTIES

5.1. Colors and Chemical Properties

Is there any correlation between the presence of a particular ice or mineralogical absorption band in the spectra of TNOs and their colors? For example, do TNOs with CH_4-ice bands in their spectra display redder surfaces than TNOs with H_2O-ice bands in their spectra? This is a reasonable correlation to study because Pluto exhibits CH_4 bands and it has a redder color than Charon, which exhibits H_2O-ice bands.

The difficulty with looking for such a correlation among TNOs is that there are only a handful of objects that are known to exhibit absorption bands in their spectra. In particular, H_2O-ice bands are seen in spectra of Charon, 1996 TO_{66} (*Brown et al.,* 1999), Varuna (*Licandro et al.,* 2001), Quaoar (*Jewitt and Luu,* 2004), Orcus (*Fornasier et al.,* 2004a), and 2003 EL_{61} and its satellite (*Barkume et al.,* 2006). CH_4-ice bands are seen in spectra of Pluto (*Cruikshank et al.,* 1976); Neptune's satellite Triton, which may be a captured TNO (*Cruikshank et al.,* 1993); Eris (*Brown et al.,* 2005); and 2005 FY_9 (*Licandro et al.,* 2006). Mineralogical bands are seen in the spectra of 2003 AZ_{84} (*Fornasier et al.,* 2004b), Huya, and 2000 GN_{171} (*Lazzarin et al.,* 2003).

Despite the small sample size, is there any correlation between the presence of CH_4, H_2O bands, and surface color? The seven TNOs exhibiting H_2O bands display colors ranging from B–V = 0.63 ± 0.03 for 2003 EL_{61} (*Rabinowitz et al.,* 2006) to B–V = 0.96 ± 0.08 for Varuna. For reference, Pluto and Charon have B–V = 0.87 ± 0.01 and B–V = 0.70 ± 0.01 (*Binzel,* 1988). The four TNOs exhibiting CH_4-ice bands and the three TNOs exhibiting mineralogical bands display a similar wide range of B–V colors. So far, there is not any obvious correlation between the presence of an ice or mineralogical band and the B–V colors of TNOs. However, larger samples may allow a better test.

5.2. Modeling of Surface Colors

What can modeling tell us about the surface colors? By comparing broadband photometric and spectroscopic observations with radiative transfer models (*Hapke,* 1981; *Douté and Schmitt,* 1998), it is possible to constrain the chemical composition of TNO surfaces. In particular, radiative transfer models make it possible to transform laboratory optical constants for candidate surface materials such as organic material (tholins and kerogen), dark material (amorphous carbon), ices, and silicates (tremolite) into reflectance spec-

tra for comparison with observations. By inputting different percentages of candidate materials in a radiative transfer model and finding the best match between the theoretical spectra and the observed spectra, it is possible to constrain the chemical composition and grain sizes on the surfaces of TNOs.

What sort of compositions do the models suggest for objects at the extreme ends of the TNO color range, i.e., a red vs. a gray TNO? It appears the observed red colors of TNOs are consistent with the presence of a tholin-like material (*Cruikshank et al.,* 1998; see also chapter by de Bergh et al.). Tholins are synthetic macromolecular compounds produced from irradiated gaseous or solid mixtures of simple hydrocarbons, water, or nitrogen (*Sagan and Khare,* 1979). Although their optical properties depend on the original mixture and conditions of irradiation, all tholins show a common characteristic, i.e., colors ranging from yellow to red. Evidently, the numerous overlapping electronic bands of these complex organic molecules produce a red pseudo-continuum at ultraviolet and optical wavelengths. *Doressoundiram et al.* (2003) find the red color, V–J = 2.44 ± 0.06, of 26181 (1996 GQ_{21}) is consistent with a mixture of 15% Titan tholin (*Khare et al.,* 1984), 35% ice tholin I (*Khare et al.,* 1993), and 50% amorphous carbon. It is important to note that such a model is only a suggestion of what might be the nature of the surface material. The solution is not unique, given the many unknown parameters in the models.

At the other extreme of color, *de Bergh et al.* (2005) found that the visible and infrared colors and spectra of the gray TNO Orcus, V–J = 1.08 ± 0.04, is consistent with a Hapke-type model that has 5% H_2O-ice at 40 K, 42% kerogen, and 53% amorphous carbon. Terrestrial kerogens are the product of decay of organic matter, but interstellar dust and some carbonaceous meteorites contain materials of similar structure of nonbiological origin. Kerogens have been used to model the spectra of some asteroids. All components in the model of Orcus had a grain size of 10 μm. For reference, the Sun has V–J = 1.08. The chapters of de Bergh et al. and Barucci et al. in this book give a more complete overview on spectral modeling and links between color properties and composition.

6. ORIGIN OF THE COLOR ANISOTROPY AND PROPOSED RESURFACING SCENARIOS

6.1. A Primordial Origin

A dynamical simulation (*Gomes,* 2003; see also chapter by Morbidelli et al.) and some thoughts on methane chemistry in the outer solar system provide a way of interpreting the colors of TNOs. The dynamical simulation predicts that as Neptune migrated outward, it scattered objects originally 25 AU from the Sun into the orbits of the present-day SDOs, high-i classical TNOs (i > 5°), and high-i Plutinos. In contrast, classical TNOs in low-e and low-i orbits (the red cluster of classical TNOs discussed in section 4) remained far enough away from Neptune that they were never perturbed much by the planet. Perhaps around 40 AU from the Sun, methane went from condensing in a water-ice rich clathrate to condensing as pure methane (*Lewis,* 1972). Whereas the loss of methane from a clathrate surface would result in a lag made up of colorless water-ice crust, a pure methane-ice crust would provide much material for alteration into red organic compounds, even if there were a substantial amount of methane sublimation. If the dynamical simulation and this idea about methane surface chemistry are correct, SDOs, high-i classical TNOs, and high-i Plutinos should exhibit gray surface colors and low-i classical TNOs should exhibit red surface colors. The SDOs are largely gray and the low-i classical TNOs are red; however, additional observations are necessary to see if the high-i classical TNOs and the high-i Plutinos are largely gray.

6.2. Evolutionary Processes

The red colors of TNOs and Centaurs are usually attributed to the effects of surface aging and darkening due to high-energy radiation and particle bombardment in interplanetary space, also called space weathering (see chapters by Hudson et al. and de Bergh et al.). Blue surface colors can be produced by major collisions with other objects through deposits of fresh icy material from the body interior or from the impactor. Smaller impacts could also refresh the surface through so-called impact gardening. Both resurfacing processes (irradiations and collisions) have very long timescales (on the order of millions of years). A complicating situation may result from a reduction of the material reddening for very intense and/or very long irradiation times. This is indicated by laboratory experiments performed on asphaltite material (*Moroz et al.,* 2003). Resurfacing on a much shorter timescale could happen due to ice recondensation and/or dust deposition from a temporary atmosphere produced by outgassing due to solar heating, and from dust coma activity. N_2 and CO ices may be able to sublimate at distances of 40 AU and beyond (*Delsemme,* 1982). This ice sublimation process works quite efficiently for Pluto, as well as possibly also for Charon (*Yelle and Elliot,* 1997) and Chiron (*Meech et al.,* 1997).

The first numerical simulation results of TNO colors were performed using simplified reddening and impact resurfacing models (*Luu and Jewitt,* 1996). The results show that the range of colors observed in TNOs can be well reproduced. Typically, red objects are exposed to high-energy radiation for a long time (on the order of 10^6 yr) without resurfacing by collision. In turn, resurfacing by collision events produces "sharp" short-term color changes to neutral or at least less red values in the objects. The modeling, and more recent work by *Delsanti et al.* (2004), did not constrain conclusively the importance of collisions in the Edgeworth-Kuiper belt. The resurfacing by ice deposits from outgassing and from high-level irradiations is viewed

as an additional "randomizing" complication of the modeling. Size- and population-dependent color modeling has not yet been performed.

7. CONCLUSION

Broadband photometry represents the simplest observing technique to study physical properties of TNOs and Centaurs. By assuming canonical albedo values together with magnitude estimates in the visible, one can get an initial idea on the typical sizes of these primitive bodies in the solar system. Color data and results derived from spectral gradient estimations provide an accurate measure of the global surface reflectance of the objects. There is no doubt that a large number of TNOs and Centaurs have very red surface colors, in fact much redder than other solar system bodies and in particular those in the inner solar system. Nevertheless, objects with neutral colors are also found.

With the large and high-quality color datasets available, strong and significant results have been found. Statistical analyses point to correlations between optical colors and orbital inclination and orbital rms velocity for the classical Edgeworth-Kuiper belt. On the other hand, no clear trend is obvious for Plutinos, scattered objects, or Centaurs, and no trend can be drawn regarding correlation of colors with size or heliocentric distance. These strong results can be summarized as follows: (1) The classical low-inclination TNOs are redder than the other populations; (2) the colors in the visible appear to be consistent throughout the visible region, but are generally unrelated to the colors in the near-IR; (3) the TNOs show strong color diversity when compared to other solar system bodies; and (4) there are color-orbital inclination and color-rms velocity correlations for the classical TNOs ($40 < a < 50$ AU).

At present, no fully convincing mechanism exists that explains the anisotropic color distribution within the Edgeworth-Kuiper disk. We do not know whether the color diversity is the result of true compositional diversity or whether it is the result of some evolutionary processes, e.g., collisions or surface irradiation processes. On the other hand, with the computational models performed so far coupled with the observational facts, we can conclude that collision alone cannot explain all, but it certainly plays a role in color distribution seen at present time in the TNOs. Not only collisions, but other evolutionary processes as well (e.g., outgassing, complex space weathering, micrometeorites, surface gardening, atmospheric interaction, etc.), have to be modeled. More observational data, numerical simulations, and overall laboratory experiments are required to unveil the origin of the color properties and trends in the present Edgeworth-Kuiper belt.

REFERENCES

Andronico G., Baratta G. A., Spinella F., and Strazzulla G. (1987) Optical evolution of laboratory-produced organics: Applications to Phoebe, Iapetus, outer belt asteroids and comet nuclei. *Astron. Astrophys., 184,* 333–336.

Bagnulo S., Boehnhardt H., Muinonen K., Kolokolova L., Belskaya I., and Barucci M. A. (2006) Exploring the surface properties of trans-neptunian objects and Centaurs with polarimetric FORS1/VLT observations. *Astron. Astrophys., 450,* 1239–1248.

Barkume K. M., Brown M. E., and Schaller E. L. (2006) Water ice on the satellite of Kuiper belt object 2003 EL_{61}. *Astrophys. J. Lett., 640,* L87–L89.

Bauer J. M., Meech K. J., Fernández Y. R., Farnham T. L., and Roush T. L. (2002) Observations of the Centaur 1999 UG_5: Evidence of a unique outer solar system surface. *Publ. Astron. Soc. Pac., 114,* 1309–1321.

Belskaya I. N. and Shevchenko V. G. (2000) Opposition effect of asteroids. *Icarus, 147,* 94–105.

Binzel R. P. (1988) Hemispherical color differences on Pluto and Charon. *Science, 241,* 1070–1072.

Boehnhardt H., Tozzi G. P., Birkle K., Hainaut O., Sekiguchi T., Vlair M., Watanabe J., Rupprech G., and the Fors Instrument Team (2001) Visible and near-IR observations of trans-neptunian objects. Results from ESO and Calar Alto telescopes. *Astron. Astrophys., 378,* 653–667.

Boehnhardt H., Delsanti A., Barucci A., Hainaut O., Doressoundiram A., Lazzarin M., Barrera L., de Bergh C., Birkle K., Dotto E., Meech K. J., Ortiz J. L., Romon J., Sekiguchi T., Thomas N., Tozzi G. P., Watanabe J., and West R. M. (2002) ESO large program on physical studies of trans-neptunian objects and Centaurs: Visible photometry — first results. *Astron. Astrophys., 395,* 297–303.

Boehnhardt H., Bagnulo S., Muinonen K., Barucci M. A., Kolokolova L., Dotto E., and Tozzi G. P. (2004) Surface characterization of 28978 Ixion (2001 KX_{76}). *Astron. Astrophys., 415,* L21–L25.

Bowell E. and Lumme K. (1979) Colorimetry and magnitudes of asteroids. In *Asteroids* (T. Gehrels, ed.), pp. 132–169. Univ. of Arizona, Tucson.

Brown R. H., Cruikshank D. P., and Pendleton Y. (1999) Water ice on Kuiper belt object 1996 TO_{66}. *Astrophys. J. Lett., 519,* L101–L104.

Brown M. E., Trujillo C. A., and Rabinowitz D. L. (2005) Discovery of a planetary-sized object in the scattered Kuiper belt. *Astrophys. J. Lett., 635,* L97–L100.

Cruikshank D. P., Pilcher C. B., and Morrison D. (1976) Pluto — Evidence for methane frost. *Science, 194,* 835–837.

Cruikshank D. P., Roush T. L., Owen T. C., Geballe T. R., de Bergh C., Schmitt B., Brown R. H., and Bartholomew M. J. (1993) Ices on the surface of Triton. *Science, 261,* 742–745.

Cruikshank D. P. and 14 colleagues (1998) The composition of Centaur 5145 Pholus. *Icarus, 135,* 389–407.

Cruikshank D. P., Imanaka H., and Dalle Ore C. M. (2005) Tholins as coloring agents on outer solar system bodies. *Adv. Space Res., 36,* 178–183.

De Bergh C., Delsanti A., Tozzi G. P., Dotto E., Doressoundiram A., and Barucci M. A. (2005) The surface of the transneptunain object 90482 Orcus. *Astron. Astrophys., 437,* 1115–1120.

Delsanti A., Hainaut O., Jourdeuil E., Meech K. J., Boehnhardt H., and Barrera L. (2004) Simultaneous visible and near-IR photometric study of Kuiper belt object surfaces with the ESO/Very Large Telescopes. *Astron. Astrophys, 417,* 1145–1158.

Delsanti A., Peixinho N., Boehnhardt H., Barucci A., Merlin F., Doressoundiram A., and Davies J. K. (2006) Near-infrared color properties of Kuiper belt objects and Centaurs: Final results from the ESO Large Program. *Astrophys. J., 131,* 1851–1863.

Degewij J. and van Houten C. J. (1979) Distant asteroids and outer

jovian satellites. In *Asteroids* (T. Gehrels, ed.), pp. 417–435. Univ. of Arizona, Tucson.

Degewij J., Cruikshank D., and Hartmann W. (1980) Near-infrared colorimetry of J7 Himalia and S9 Phoebe: A Summary of 0.3 to 2. m reflectances. *Icarus, 44,* 541–547.

Delsemme A. H. (1982) Chemical composition of cometary nuclei. In *Comets* (L. L. Wilkening, ed.), pp. 85–130. Univ. of Arizona, Tucson.

Doressoundiram A. and Boehnhardt H. (2003) Multicolour photometry of trans-neptunian objects: Surface properties and structures. *Compt. Rend. Phys., 7,* 755–766.

Doressoundiram A., Barucci M. A., Romon J., and Veillet C. (2001) Multicolor photometry of trans-neptunian objects. *Icarus, 154,* 277–286.

Doressoundiram A., Peixinho N., De Bergh C., Fornasier S. Thebault Ph., Barucci M. A., and Veillet C. (2002) The color distribution of the Kuiper belt. *Astron. J., 124,* 2279–2296.

Doressoundiram A., Tozzi G. P., Barucci M. A., Boehnhardt H., Fornasier S., and Roman J. (2003) ESO large programme on trans-neptunian objects and Centaurs: Spectroscopic investigation of Centaur 2001 BL_{41} and TNOs (26181) 1996 GQ_{21} and (26375) 1999 DE_9. *Astron. J., 125,* 2721–2727.

Doressoundiram A., Peixinho N., Doucet C., Mousis O., Barucci M. A., Petit J. M., and Veillet C. (2005) The Meudon multicolor survey (2MS) of Centaurs and trans-neptunian objects: Extended dataset and status on the correlations reported. *Icarus, 174,* 90–104.

Douté S. and Schmitt B. (1998) A multilayer bi-directional reflectance model for the analysis of planetary surface hyperspectral images at visible and near-infrared wavelengths. *J. Geophys. Res., 103,* 31367–31390.

Fornasier S., Dotto E., Barucci M. A., and Barbieri C. (2004a) Water ice on the surface of the large TNO 2004 DW. *Astron. Astrophys., 422,* L43–L46.

Fornasier S., Doressoundiram A., Tozzi G. P., Barucci M. A., Boehnhardt H., de Bergh C., Delsanti A., Davies J., and Dotto E. (2004b) ESO large program on physical studies of trans-neptunian objects and Centaurs: Final results of the visible spectrophotometric observations. *Astron. Astrophys., 421,* 353–363.

French L. M. and Binzel R. P. (1989) CCD photometry of asteroids. In *Asteroids II* (R. P. Binzel et al., eds), pp. 54–65. Univ. of Arizona, Tucson.

Glass I. S. (1997) *Handbook of Infrared Astronomy.* Cambridge Univ., Cambridge.

Gomes R. S. (2003) The origin of the Kuiper belt high-inclination population. *Icarus, 161,* 404–418.

Gradie J. and Tedesco E. (1982) Compositional structure of the asteroid belt. *Science, 216,* 1405–1407.

Gradie J. and Veverka J. (1980) The composition of the Trojan asteroids. *Nature, 283,* 840–842.

Hainaut O. R. and Delsanti A. C. (2002) Colors of minor bodies in the outer solar system. *Astron. Astrophys., 389,* 641–664.

Hapke B. (1981) Bidirectional reflectance spectroscopy. 1. Theory. *J. Geophys. Res., 86,* 3039–3054.

Hardorp J. (1980) The sun among the stars. III — Energy distribution of 16 northern G-type stars and solar flux calibration. *Astron. Astrophys., 91,* 221–232.

Hartmann W. K., Cruikshank D. P., and Degewij. J. (1982) Remote comets and related bodies — VJHK colorimetry and surface materials. *Icarus, 52,* 377–409.

Howell S. B. (1989) Two-dimensional aperture photometry — Signal-to-noise ratio of point-source observations and optimal data-extraction techniques. *Publ. Astron. Soc. Pac., 101,* 616–622.

Jewitt D. and Luu J. (1993) Discovery of the candidate Kuiper belt object 1992 QB_1. *Nature, 362,* 730–732.

Jewitt D. and Luu J. X. (2001) Colors and spectra of Kuiper belt objects. *Astron. J., 122,* 2099–2114.

Jewitt D. C. and Luu J. (2004) Crystalline water ice on the Kuiper belt object (50000) Quaoar. *Nature, 432,* 731–733.

Khare B. N., Sagan C., Arakawa E. T., Suits F., Callcott T. A., and Williams M. W. (1984) Optical constants of organic tholins produced in a simulated titanian atmosphere — from soft X-ray to microwave frequencies. *Icarus, 60,* 127–137.

Khare B. N., Thompson W. R., Cheng L., Chyba C., Sagan C., Arakawa E. T., Meisse C., and Tuminello P. S. (1993) Production and optical constants of ice tholin from charged particle irradiation of (1:6) C_2H_6/H_2O at 77K. *Icarus, 103,* 290–300.

Lazzarin M., Barucci M. A., Boehnhardt H., Tozzi G. P., de Bergh C., and Dotto E. (2003) ESO large programme on physical studies of trans-neptunian objects and Centaurs: Visible spectroscopy. *Astron. J., 125,* 1554–1558.

Lewis J. S. (1972) Low temperature condensation from the solar nebula. *Icarus, 16,* 241.

Licandro J., Oliva E., and Di Martino M. (2001) NICS-TNG infrared spectroscopy of trans-neptunian objects 2000 EB_{173} and 2000 WR_{106}. *Astron. Astrophys., 373,* L29–L32.

Licandro J., Pinilla-Alonso N., Pedani M., Oliva E., Tozzi G. P., and Grundy W. M. (2006) The methane ice rich surface of large TNO 2005 FY9: A Pluto-twin in the trans-neptunian belt? *Astron. Astrophys., 445,* L35–L38.

Luu J. and Jewitt D. (1996) Color diversity among the Centaurs and Kuiper belt objects. *Astrophys. J., 112,* 2310.

McCord T. B. and Chapman C. R. (1975) Asteroids — Spectral reflectance and color characteristics. *Astrophys. J., 195,* 553–562.

Meech K. J., Buie M. W., Samarasinha N. H., Mueller B. E. A., and Belton M. J. S. (1997) Observations of structures in the inner coma of Chiron with the HST Planetary Camera. *Astrophys. J., 113,* 844–862.

Moore M. H., Donn B., Khanna R., and A'Hearn M. F. (1983) Studies of proton-irradiated cometary-type ice mixtures. *Icarus, 54,* 388–405.

Moroz L. V., Baratta G., Distefano E., Strazzulla G., Starukhina L. V., Dotto E., and Barucci M. A. (2003) Ion irradiation of asphaltite: Optical effects and implications for trans-neptunian objects and Centaurs. *Earth Moon Planets, 92,* 279–289.

Mueller B. E. A., Tholen D. J., Hartmann W. K., and Cruikshank D. P. (1992) Extraordinary colors of asteroidal object (5145) 1992 AD. *Icarus, 97,* 150–154.

Peixinho N., Doressoundiram A., Delsanti A., Boehnhardt H., Barucci M. A., and Belskaya I. (2003) Reopening the TNOs color controversy: Centaurs bimodality and TNOs unimodality. *Astron. Astrophys., 410,* L29–L32.

Rabinowitz D. L., Barkume K., Brown M. E., Roe H. S. M., Tourtellotte S., and Trujillo C. (2006) Photometric observations constraining the size, shape, and albedo of 2003 EL_{61}, a rapidly rotating, Pluto-sized object in the Kuiper belt. *Astrophys. J., 639,* 1238–1251.

Russell H. N. (1916) On the albedo of the planets and their satellites. *Astron. J., 43,* 173.

Sagan C. and Khare B. N. (1979) Tholins — Organic chemistry of interstellar grains and gas. *Nature, 277,* 102–107.

Sheppard S. S. and Jewitt D. C. (2002) Time-resolved photometry of Kuiper belt objects: Rotations, shapes and phase functions. *Astron. J., 124,* 1757–1775.

Spearman C. (1904) The proof and measurement of association between two things. *Am. J. Psych., 57,* 72–101.

Sterken C. and Manfroid J. (1992) *Astronomical Photometry — A Guide.* Astrophys. Space Sci. Library, Kluwer, Dordrecht.

Stern S. A. (2002) Evidence for a collisional mechanism affecting Kuiper belt object colors. *Astron. J., 124,* 2297–2299.

Strazzulla G., Cataliotti R. S., Calcagno L., and Foti G. (1984) The IR spectrum of laboratory synthesized polymeric residues. *Astron. Astrophys., 133,* 77–79.

Tegler S. C. and Romanishin W. (1997) The extraordinary colors of trans-neptunian objects 1994 TB and 1993 SC. *Icarus, 126,* 212–217.

Tegler S. C. and Romanishin W. (1998) Two distinct populations of Kuiper-belt objects. *Nature, 392,* 49.

Tegler S. C. and Romanishin W. (2000) Extremely red Kuiper-belt objects in near-circular orbits beyond 40 AU. *Nature, 407,* 979–981.

Tegler S. C., Romanishin W., and Consolmagno G. J. (2003) Color patterns in the Kuiper belt: A possible primordial origin. *Astrophys. J. Lett., 599,* L49–L52.

Trujillo C. A. and Brown M. E. (2002) A correlation between inclination and color in the classical Kuiper belt. *Astrophys. J. Lett., 566,* L125–L128.

Yelle R. V. and Elliot J. L. (1997) Atmospheric structure and composition: Pluto and Charon. In *Pluto and Charon* (S. A. Stern and D. J. Tholen, eds.), p. 347. Univ. of Arizona, Tucson.